HHS Public Access

Author manuscript

Nat Neurosci. Author manuscript; available in PMC 2015 November 01.

Published in final edited form as:

Nat Neurosci. 2015 May ; 18(5): 728–735. doi:10.1038/nn.3998.

Mesopontine median raphe regulates hippocampal ripple oscillation and memory consolidation

Dong V. Wang, **Hau-Jie Yau**, **Carl J. Broker**, **Jen-Hui Tsou**, **Antonello Bonci**, and **Satoshi Ikemoto**

Intramural Research Program, National Institute on Drug Abuse, National Institutes of Health, Baltimore, Maryland 21224, USA

Abstract

Sharp-wave associated field-oscillations (~200 Hz) of the hippocampus, referred to as “ripples”, are believed to be important for consolidation of explicit memory. Little is known about how ripples are regulated by other brain regions. Here we show that the median raphe region (MnR) plays a key role in regulating hippocampal ripple activity and memory consolidation. We performed *in vivo* simultaneous recording in the MnR and hippocampus, and found that when a group of MnR neurons were active, ripples were absent. Consistently, optogenetic stimulation of MnR neurons suppressed ripple activity, while inhibition of these neurons increased ripple activity. Importantly, using a fear conditioning procedure, we provided evidence that photostimulation of MnR neurons interfered with memory consolidation. Our results demonstrate a critical role of the MnR in regulating ripples and memory consolidation.

Memory consolidation, a process that transforms newly acquired information into long-term memory, depends critically on the hippocampus [1,2]. The hippocampus generates ripple activity, a sharp-wave associated fast field-oscillation (100–300 Hz), which is predominantly detected in the CA1 region [3–5]. Converging evidence suggests that ripple activity reflects memory consolidation process [6]. Previous studies have shown that firing of hippocampus place cells during locomotor navigation are subsequently “replayed” in the same sequence, but in a temporary compressed manner [7–9], and importantly, the replay coincides with ripples [9,10]. Moreover, selective disruption of ripple activities after learning trials of a task results in poor performance of the task, an effect likely caused by disrupted

Corresponding author: Satoshi Ikemoto, Behavioral Neuroscience Research Branch, National Institute on Drug Abuse, National Institutes of Health, 251 Bayview Blvd., Suite 200, Baltimore, MD 21224, USA, Tel: (443) 740-2722, Fax: (443) 740-2827, Satoshi.Ikemoto@nih.gov.

The authors declare no competing financial interest in relation to the present paper.

Author Contributions

D.V.W., H.Y. and S.I. designed the experiments; D.V.W., H.Y., C.J.B. and J.T. performed the experiments; D.V.W. analyzed the data with help from H.Y., C.J.B. and J.T.; D.V.W., H.Y., A.B. and S.I. contributed to interpretation of the data; and D.V.W. and S.I. wrote the paper.

Author Information

The authors declare no competing financial interests.

A supplementary methods checklist is available.

memory consolidation [10–12]. Ripple activity frequently occurs during inattentive states including slow-wave sleep, awake immobility and feeding [13,14]. However, little is known about how ripple activity is regulated.

A recent study reported that hippocampal ripple activity is accompanied by inhibition of subcortical regions [15]. This observation raises a question whether subcortical regions play any role in regulating ripple activity. The median raphe region (MnR), localized along the midline of the ventral mesopontine area, projects extensively to the forebrain and has been implicated in regulation of state [16]. Importantly, MnR neurons project to the entire hippocampal formation [17–20] and participate in regulation of hippocampal theta activity [21] and thereby possible regulation of learning and memory [22,23]. The present study reports that activation of MnR neurons suppresses hippocampal ripple activity and disrupts memory consolidation.

RESULTS

MnR neurons display hippocampal ripple correlated activity

To investigate whether and how the MnR is involved in regulating hippocampal neural activity, we implanted a bundle of 8 tetrodes in the MnR and another 4 tetrodes in the hippocampal CA1 region of C57BL/6J mice (Fig. 1a). The tetrodes were coupled with miniature micro-drives to achieve precise placement in the targeted CA1 pyramidal layer in the hippocampus (Supplementary Fig. 1a–c). In addition, it allowed us to record neural activity at several different depths within the MnR by driving the tetrodes down (~80 μm advancement per step), resulting in a higher yield in the total number of recorded MnR neurons (see Methods). We simultaneously recorded local field potentials (LFP) and single neuron activity in the hippocampal CA1 and MnR in freely-behaving mice (i.e., without restrain or anesthesia) in their homecages, and analyzed neural data recorded when the mice were in a quiet immobile state that likely corresponded to slow-wave sleep (referred to as “immobile/sleep”; see Methods and Supplementary Fig. 1d,e), unless otherwise noted. Hippocampal ripple activity was band-pass filtered at 150–250 Hz, and ripple events were identified with peak amplitude exceeding 6 standard deviations of baseline activity (Fig. 1b; see Methods).

We recorded a total of 191 MnR neurons from 6 mice (see Supplementary Fig. 2a,b for electrodes placements) and first identified serotonergic and non-serotonergic neurons. About 15% (29/191; maintained firing rate = 1.34 ± 0.97 Hz, mean ± s.d.) were classified as putative serotoninergic neurons according to established criteria (Supplementary Fig. 2c–f; see Methods). Consistent with previous studies, these classified serotonin neurons displayed a slow, steady firing rate (i.e., long inter-spike intervals), which was suppressed by administration of a serotonin 1A receptor agonist (Supplementary Fig. 2e). We then examined the timing of putative serotonin neuron firing relative to hippocampal ripple activity, and found that the majority (22/29) showed a small but significant decrease in activity coinciding with ripple events (Fig. 1c, d, left panels; peri-event histogram trough z-score < −3.28 and $P < 0.001$, Wilcoxon signed-rank test).

In addition, we classified non-serotonergic neurons with respect to their activity and hippocampal ripples. The majority of non-serotonergic MnR neurons (59%, 96/162) displayed significant ripple-correlated activity changes (Fig. 1c, d; peri-event histogram z-score absolute value > 3.28 and $P < 0.001$, Wilcoxon signed-rank test), and these neurons were further divided into two types. Type-I neurons (43%, 41/96; 2.4 ± 1.7 Hz, mean ± s.d.) displayed a prolonged decrease in activity (80% of baseline or lower) that lasted 1 s or longer prior to ripple events (Fig. 1c, d, middle panels and Supplementary Fig. 2g). Immediately after ripple events, about half of them transiently restored their firing rates to baseline or higher. On the other hand, type-II neurons (57%, 55/96; 14.2 ± 12.3 Hz) displayed a diversity of robust transient activity (inhibitory, excitatory or both) that coincides with ripple events, while having little change in firing frequency before ripple events (Fig. 1c, d, right panels and Supplementary Fig. 2g); therefore, they appear to be a heterogeneous collection of neurons. As noted above, ripple activity is present during feeding. The ripple-correlated type-I neural activity during feeding differs from that of immobile/sleeps state (Supplementary Fig. 3b). During feeding, type-I neurons were inhibited less before ripple event and excited more immediately after ripple event.

Rates and synchrony of type-I neuron firing during ripple events

The key feature that type-I neurons are silent just prior to the occurrence of ripple events (Fig. 1c, d, middle panels) raises the question of whether suppression of type-I neuron activity is a necessary condition for hippocampal ripples to occur; in other words, is activation of these neurons likely to suppress ripple events? To examine this intriguing possibility, we analyzed the raw data of spike trains of type-I neurons with respect to ripple events. The absence of ripple activity was usually accompanied by increased firing rates of type-I neurons (Fig. 2a). Because inter-spike intervals (ISIs) varied extensively among type-I neurons (Supplementary Fig. 4a,b), we first examined ripple activity when type-I neuron firing-rates increased 2-fold above their mean firing-rates (“high” instant rate; Fig. 2b and Supplementary Fig. 4c). We found that ripple activity was largely suppressed when firing rates of type-I neurons increased 2-fold or greater (Fig. 2c). The temporal relationship between type-I neuron activity and ripple events was also verified by additional auto-correlation and cross-correlation analyses (Fig. 2d and Supplementary Fig. 4d,e). Notably, type-I neurons fired immediately after a transient increase of ripple activity (Fig. 2c,d), raising the possibility that the post-ripple firing of type-I neurons may be recruited for immediate suppression of subsequent ripple activity. In addition, we created a smoothed firing rate estimate for each type-I neuron and a smoothed rate estimate for ripple events. Type-I neuron firing rates were averaged every 500-ms epoch and then scatter-plotted with the corresponding ripple rates (Fig. 2e). Our analyses show that hippocampal ripple activity was strongly suppressed for a few seconds after fast firing of the type-I neuron (Fig. 2f,g).

In addition, MnR type-I neurons fired in synchrony during immobile/sleep state (Fig. 3a), and a cross-correlation analysis confirmed strong synchronous firings among all the simultaneously recorded type-I neurons (Fig. 3b,c; cross-correlation histogram peak z-score > 3.28 and $P < 0.001$, Wilcoxon signed-rank test). The averaged cross-correlation histogram shows that most of the synchronized firings are within a time window of less than 200 ms (Fig. 3d). To determine how the co-firing within different size windows relates to ripple

events, we divided the spikes of each type-I neuron into five sets based on the co-firing interval (i.e., the interval of the closest co-fired spikes; Fig. 3e), with a smaller co-firing interval indicating a higher synchrony. We found that the more synchronized firing between type-I neurons, the larger suppression of the ripple activity (Fig. 3e,f). These results suggest that MnR type-I neurons strongly suppress hippocampal ripple activity by coordinating firings among themselves. In addition, we found that the MnR serotonergic neurons also synchronize with the type-I neuron, though mostly with a brief ~200–300 ms delay (Supplementary Fig. 5).

Hippocampal ripples tend to occur in clusters (Supplementary Fig. 6a,b). We therefore examined how type-I neural activity may correlate with the ripple clusters, specifically the onsets and offsets of ripple clusters. Our analyses revealed that the greater the frequency of type-I neuron firing, the more synchronized the firings of MnR type-I neurons at the offset rather than onset of ripple clusters (Supplementary Fig. 6c–f), while low firing-rates and unsynchronized firing showed little or no difference in relationship to the onset and offset of ripple clusters (Supplementary Fig. 6c–f). Thus, increased firing-rates and increased synchronicity of type-I neurons predict the presence of streaks of ripple activity and may be needed to suppress them.

Up- and down-regulation of ripple activity by MnR neurons

To determine a causal relationship between MnR neuron firing and ripple suppression, we employed an optogenetic approach. We injected a serotype-1 adeno-associated viral (AAV1) vector encoding channelrhodopsin-2 (ChR2) fused with enhanced yellow fluorescent protein (EYFP), driven by a general *synapsin* promoter, into the MnR. An optic fiber was then implanted in the dorsal portion of the MnR, while a bundle of 4 tetrodes were implanted in the hippocampal CA1 layer to record ripple and single-neuron activities (Fig. 4a,b). After a post-operation period of 3 weeks, which allowed sufficient somatic expression of ChR2 in the MnR, we examined effects of MnR photostimulation (473 nm blue light) on hippocampal neural activity. We delivered a pair of 3-ms pulse photostimulation (25 Hz) into the MnR with a variable interval schedule of 10 s (randomly varied between 5 and 15 s) during immobile/sleep state, and found that hippocampal ripple activities were nearly abolished for 1 s (Fig. 4c). Consistently, the vast majority of the recorded CA1 neurons (93%; 57/61) showed a significant change in activity (peri-event histogram z-score absolute value > 3.28 and $P < 0.001$, Wilcoxon signed-rank test), both positive and negative, upon MnR photostimulation (Fig. 4d; see Supplementary Fig. 7 for the characterization of CA1 neurons), suggesting that MnR neurons strongly regulate hippocampal CA1 neural activity. We also examined effects of MnR neuron inhibition with intra-MnR AAV encoding halorhodopsin (eNpHR3.0) during immobile/sleep state, and found that photoinhibition (2-s continuous 532-nm light) of the MnR neurons significantly increased hippocampal ripple activity from the baseline, followed by a significant rebounding decrease in ripple activity below the baseline (Fig. 4e; one-way repeated ANOVA with the three 2-s blocks, $F_{2, 8} = 25.34$, $P = 0.0004$, followed by Tukey's HSD posthoc test, $P < 0.05$).

Moreover, subset of CA1 neurons displayed firing changes during and after MnR photoinhibition (Fig. 4f). Together, these results show that the MnR manipulations are

capable of up- and down-regulation of the ripple activity, which thus strongly support our hypothesis that the MnR plays a critical role in regulating hippocampal ripple activity.

Subtypes of MnR neurons in regulation of ripple activity

The MnR contains heterogeneous populations of neurons with respect to neurotransmitters[24,25], and transmitter heterogeneity may help to explain the activity heterogeneity we observed (Fig. 1c, d). To begin to determine which specific type of MnR neurons mediates the long-lasting suppression of hippocampal ripple activity, we delivered Cre-dependent AAV vectors encoding ChR2-EYFP into the MnR of ePet-Cre[26] and Vgat-IRES-Cre[27] transgenic mice to selectively stimulate serotonergic and GABAergic neurons, respectively. We first verified the specificity of viral infection (Fig. 5a,c): 96.2% (512/532; n = 3 mice) of EYFP-positive neurons were positive for tryptophan hydroxylase (TPH) in ePet-Cre mice, and 94.6% (560/592; n = 2 mice) of EYFP neurons are positive for glutamic acid decarboxylase (GAD) mRNA in Vgat-IRES-Cre mice. Also, the viral infection efficiencies were relatively high: 67.4% (512/760) of the TPH-positive neurons and 74.4% (560/753) of the GAD-positive neurons were EYFP-positive, respectively. Next, we confirmed that the infected neurons respond to photostimulation in slice recordings (Fig. 5b,d). *In vitro* slice recording were conducted in EYFP-positive MnR neurons. Both serotonergic (n = 5) and GABAergic (n = 6) neurons responded to a 200-ms continuous blue light (Fig. 5b,d, top panels). While all GABAergic neurons (n = 6) responded to every light pulse of a 4-pulse train (25 Hz; pulse width, 3 ms), only 3 out of 5 serotonergic neurons were able to respond to every light pulse (Fig. 5b,d, bottom panels), and the other 2 serotonergic neurons only fired one single spike.

To examine the role of individual MnR populations in ripple regulation, we used multiple parameters, including 1, 2, 4 and 25 pulses of 3-ms blue light for MnR photostimulation *in vivo* (Fig. 5e). Consistent with our results above (Fig. 1c,d, left panels), photostimulation of serotoninergic neurons resulted in moderate reduction of CA1 ripple activities compared to non-selective MnR photostimulation (Fig. 5f,g). Photostimulation of MnR GABAergic neurons resulted in a rebound suppression of ripple activity at the termination of photostimulation (Fig. 5h), suggesting that the MnR GABAergic neurons indirectly regulate ripple activity by inhibiting MnR non-GABAergic neurons. These above results suggest that the MnR serotoninergic or GABAergic neurons alone play partial or minor roles in regulating hippocampal ripple activity.

To directly examine neurochemical identity of the three neural types (Fig. 1c,d), we employed an optogenetic tagging approach (Fig. 6). First, we injected the Cre-dependent ChR2 virus into the MnR of ePet-Cre or Vgat-IRES-Cre mice. We then implanted an optetrode (an optical fiber combined with 4 tetrodes) in the MnR and another 4-tetrode bundle in the CA1 (Fig. 6a). The optetrodes allowed us to determine with subsequent photostimulation whether recorded neurons had been serotonergic or GABAergic. Our results show that most of the classified putative 5-HT neurons were indeed serotonergic (Fig. 6b,c,f), confirming that our classification criteria for MnR 5-HT neurons are valid (Supplementary Fig. 2c–f). On the other hand, the majority of the type-II neurons were GABAergic (Fig. 6d–f). However, the MnR type-I neurons were mostly not serotonergic or

GABAergic (Fig. 6f). These results are consistent with our above results showing that the MnR serotoninergic and GABAergic neurons play partial or minor roles in regulating hippocampal ripple activity (Fig. 5f–h).

Impairment of fear memory by MnR photostimulation

The interruption of hippocampal ripple activity has been shown to disrupt memory consolidation as indicated by poor performance of memory-guided behaviour[10,11,28]. To determine whether MnR photostimulation that suppressed hippocampal ripple activity would disrupt memory consolidation, we employed a hippocampus-dependent contextual fear conditioning procedure[29,30]. Mice received MnR injections of either ChR2-EYFP or EYFP vector driven by the *synapsin* promoter and an optic-fiber implantation for subsequent photostimulation (see Supplementary Fig. 8 for fiber placements). Three weeks later, the mice were habituated to the conditioning chamber for 10 min; the next day, they received footshock (0.8 mA, 2 s) in the chamber, followed by a 4-h session with photostimulation (2 pulses per 2 s only if mice were immobile; for ripple suppression efficiency see Supplementary Fig. 9a) in their homecage; and on day 3, they were tested for freezing behavior in the chamber (Fig. 7a). ChR2-EYFP-expressing mice displayed significantly less conditioned freezing than EYFP-expressing control mice (Fig. 7f; $P = 0.0042$, unpaired t-test). This result does not appear to result from possible neural damage caused by photostimulation (Supplementary Fig. 9c,d) or possible sleep cycle dysregulation. Both SWS and REM sleep were preserved (Fig. 7b,c and Supplementary Fig. 10) with a slight increase in REM sleep (Supplementary Fig. 9b) and a decrease in SWS delta (1–4 Hz) power ($P = 1.3 \times 10^{-6}$, unpaired t-test; Fig. 7c, top panel), which is probably due to the reduction of ripple-associated sharp-waves (~2–3 Hz). Consistently, during the 4-h photostimulation session, the total immobility time did not differ between the two groups (Fig. 7d; $P = 0.696$, unpaired t-test). The two groups did not show a significant difference in freezing response before the fear conditioning (Fig. 7e; $P = 0.364$, unpaired t-test), either. These results suggest that MnR photostimulation immediately after fear conditioning impairs memory consolidation processes.

DISCUSSION

We found that many MnR neurons were inactive when hippocampal ripple events occur during immobile/sleep state. MnR serotonin neurons were inactive just prior to ripple events; however, this effect was generally small. Our observation that many of non-serotonergic neurons displayed prolonged suppression just prior to ripple events led us to the hypothesis that firing of those (type-I) neurons suppresses ripple events. Consistent with the hypothesis, we found that the greater became the firing rate and synchronicity of MnR type-I neurons, the stronger became the suppression of ripple events. Moreover, we observed that optogenetic excitation and inhibition of MnR neurons suppressed and enhanced ripple activity, respectively. Selective excitation of serotonin neurons had small effects. While selective excitation of GABA neurons had little effect, prolonged inhibition of GABA neurons was followed by clear rebound suppression of ripple activity, raising a question whether GABA neurons inhibit type-I neurons. Finally, we found that optogenetic

stimulation of MnR neurons after fear conditioning disrupted the acquisition of conditioned fear response, suggesting interference in memory consolidation.

Roles of MnR neurons in suppression of ripple activity

It is important to note that MnR type-I neurons fire immediately after ripple event (Fig. 1c,d). This observation implies that type-I neurons receive information regarding hippocampal activity. In other words, the activity of type-I neurons appears to be regulated in relation to ripple events. This implication raises two important questions: how type-I neuron activity is coordinated in relation to ripple events. This question may not be easy to answer since there is no direct projection from the hippocampal formation to the MnR. In addition, what function does such interaction serve? The activity of type-I neurons may be characterized as insertion of a “gap” between ripple events, and consequently, it may be pacing memory consolidation.

The previous finding that stimulation of serotonergic neurons produces a rapid excitation of hippocampal interneurons [19,31] may have suggested a significant contribution of serotonergic neurons for the suppression of ripple activity. However, our results suggest that MnR serotonergic neurons do not readily suppress hippocampal ripple activity: First, serotonergic neurons were inhibited just prior to ripple events to a lesser extent than type-I neurons. In addition, selective excitation of serotonergic neurons suppressed ripple activity much less effectively than non-selective excitation of MnR neurons. Our electrophysiological criteria for identifying serotonin neurons were confirmed with pharmacological and optogenetic tests. Injections of the 5-HT_{1A} receptor agonist 8-OH-DPAT inhibited serotonergic neurons identified by the electrophysiological criteria (Supplementary Fig. 2c,d). Moreover, none of type-I or II neurons responded to optogenetic stimulation that selectively excited serotonin neurons (Fig. 6f). However, we cannot conclude that serotonergic neurons play little role in ripple suppression, since our procedures were not completely irrefutable. Our optogenetic procedure involving ePet-Cre mice resulted in viral expression in 67% of MnR serotonergic neurons; therefore, we cannot exclude the possibility that some unaffected serotonergic neurons would have effectively suppressed ripple activity. In addition, our electrophysiological recording procedure may have missed, for unknown reasons, those serotonergic neurons with prolonged inhibition prior to ripple events.

In any case, it is clear that non-serotonergic neurons play an important role in suppressing hippocampal ripple activity. Since the majority of type-I neurons are not serotonergic or GABAergic, they may be glutamatergic neurons. The majority of MnR neurons projecting to the hippocampus contain vesicular glutamate transporter type 3 (VGlut3) [24,32–34]. Indeed, previous studies have shown that the stimulation of MnR neurons excites hippocampal interneurons with a short latency, its synapses contain glutamate receptors, and its excitatory effect was blocked by glutamate receptor antagonists [19,34]. Given those and the present findings, it is reasonable to hypothesize that type-I neurons are largely glutamatergic.

Roles of the MnR in memory consolidation

We provided evidence, using a fear conditioning procedure, that MnR neurons play an important role in memory consolidation via interrupting hippocampal ripple activity. Although the present study focused on MnR neural activity in relation to hippocampal ripple activity, the MnR may regulate memory consolidation through its projections to thalamocortical regions as well. Interactions between the hippocampus, thalamus and cortical regions, including the medial prefrontal cortex, during slow-wave sleep are thought to be critical for memory consolidation [35–38]. Spindles are low-frequency oscillations generated by the reticular thalamic neurons [37], and are detected in the medial prefrontal cortex whose spindles occur close in time with hippocampal ripples [39]. MnR neurons project directly to the medial prefrontal cortex [18] and extensively to the midline thalamic regions including the reuniens, mediodorsal, paracentral, parafascicular, central lateral and central medial nuclei [18], which in turn, project to the medial prefrontal cortex [40]. These MnR projections may participate in regulation of memory consolidation, in addition to its projection to the hippocampus.

Roles of MnR in hippocampal functions and behavioral state

The MnR is involved in suppression of hippocampal theta oscillation, and its mechanism differs from that in suppression of ripple activity. Stimulation of the MnR desynchronizes hippocampal LFPs [41–46], whereas lesions of the MnR [43,44] or pharmacological manipulations that inactivate MnR neurons [47–49] elicit hippocampal theta oscillations. Serotonergic neurons appear to play an important role in suppressing hippocampal theta activity. Stimulation of MnR serotonergic autoreceptors inactivates serotonergic neurons and elicits hippocampal theta oscillations [49]. Conversely, lesion-induced theta-oscillations are readily abolished by injections of the 5-HT precursor L-5-hydroxytryptophan [44]. Similarly, the 5-HT synthesis inhibitor *p*-chlorophenylalanine disrupts MnR-stimulation induced desynchronized LFPs in the hippocampus [41]. In addition, suppression of hippocampal theta oscillations by MnR neurons appears to be mediated by the medial septum/diagonal band of Broca (MS/DB), which is involved in the generation of hippocampal theta rhythm [41]. MnR stimulation disrupts rhythmical discharge of MS/DB neurons. Conversely, inhibition of serotonergic neurons with intra-MnR injections of 8-OH-DPAT elicits rhythmical discharge in MS/DB neurons synchronized with hippocampal theta activity [50]. In summary, theta suppression involves serotonergic neurons projecting through the MS/DB, while ripple suppression largely involves non-serotonergic, most likely glutamatergic, neurons projecting through direct pathways.

Interestingly, we found that the firing of serotonergic neurons was correlated with that of type-I neurons (Supplementary Fig. 5). While significance of this observation has not yet been determined, it may indicate that the MnR regulates processes involving multiple forebrain regions, including the hippocampus and MS/DB, for coordinated global functions. It is also possible that serotonergic neurons work together with type-I neurons in suppressing ripple activity. In addition to cognitive functions involving the hippocampus and MS/DB, the MnR is involved in tonically suppressing motivated behaviors. The inhibitory manipulations of local MnR neurons that elicit hippocampal theta activity in anesthetized animals also induce feeding, drinking, reward-seeking and reward [16]. While downstream

neural mechanisms involved in cognitive and motivational processes may be markedly different, the MnR appears to regulate environmental stimuli and behavior.

In conclusion, the present study found that the MnR plays a critical role in regulating hippocampal ripple oscillation and memory consolidation, and thereby provides a fundamentally new perspective on the role of subcortical regions in hippocampal functions. The present finding stimulates a new line of research, and may lead to new insights for treatments of affective/anxiety disorders arising from dysregulated memory processes.

ONLINE METHODS

Mice

Male C57BL/6J mice (3–5 month old; from Jackson Laboratories), ePet-Cre[26] and Vgat-IRES-Cre[27] mice crossed with C57BL/6J (3–5 month old; NIDA animal facility) were used. After surgery, they were singly housed in a plastic cage (30×20×20 cm) containing woodchips and cotton material and kept on a 12 h light/dark cycle and had *ad libitum* access to food and water except during testing. All procedures were approved by the Animal Care and Use Committee of the Intramural Research Program, National Institute on Drug Abuse (NIDA) and were in accordance with National Research Council's *Guide for the Care and Use of Laboratory Animals*.

Viral vectors

The NIDA Optogenetics and Transgenic Technology Core produced adeno-associated virus serotype-1 (AAV1) encoding channelrhodopsin-2 (ChR2), halorhodopsin (eNpHR-3.0) and enhanced yellow fluorescent protein (EYFP): AAV1-hSyn-hChR2 (H134R)-EYFP, AAV1-hSyn-(eNpHR-3.0)-EYFP and AAV1-hSyn-EYFP (control vector). The final viral concentration was ~ 10^{12} GC/ml. The University of Pennsylvania Penn Vector Core produced Cre-dependent AAV encoding ChR2 and EYFP, the pAAV-Ef1a-DIO-hChR2 (H134R)-EYFP-WPRE-hGH and pAAV-Ef1a-DIO-EYFP-WPRE-hGH. The final viral concentration was 9×10^{12} GC (genome copies)/ml.

Stereotaxic surgery

Mice were anesthetized with ketamine/xylazine mixture (~80/12 mg/kg, i.p.). Some mice received a bundle of electrodes implanted in the hippocampal CA1, while others received two bundles of electrodes implanted in the CA1 and MnR, consisting of the median and paramedian raphe nuclei. The coordinates for the MnR were AP –4.5 mm posterior from Bregma, ML 0.4 mm lateral from midline, DV 3.9 mm ventral from the dorsal surface of the brain, tilted with a 6-degree angle on a coronal plane with the tip pointing toward the midline (to avoid sinus); the coordinates for CA1 were AP –2.3 mm, ML 1.8 mm and DV 1.1 mm in the right hemisphere. The electrode bundles were slowly lowered toward the MnR and CA1, respectively, and secured on the skull with stainless screws and dental cement. After ~3 days recovery from surgery, electrodes were screened for neural activity.

The coordinates for MnR viral injections are AP –4.5 mm, ML 0.0 mm, DV 4.2 mm. AAV viral vectors (0.25 or 0.5 μl) was microinjected into the MnR with a syringe pump (Micro 4,

World Precision Instruments) over 5 or 10 min, with additional 10 min before removal of the injection needle (34 gauge, beveled). An optic fiber (200-μm diameter) or an optetrode (100-μm diameter optical fiber glued together with 4 tetrodes) was then chronically implanted 0.2 mm dorsal to the injection site, and was secured on the skull with stainless screws and dental cement. Experiments were started 3–4 weeks after surgery, to allow gene expression.

Immunohistochemistry

Tryptophan hydroxylase (TPH) straining—Three weeks after receiving an AAV1-DIO-EYFP injection, 3 mice were intracardially perfused with ice-cold 0.9% saline followed by 4% paraformaldehyde. Brains were coronally sectioned with a 30-μm thickness, and then TPH was visualized with a rabbit anti-TPH (1:500; Product No. T0678, Sigma) and a donkey anti-mouse secondary antibody (1:50; Code No. 715-025-151, Jackson ImmunoResearch laboratories Inc.). Mounted sections were counterstained with DAPI (4′,6-diamidino-2-phenylindole), a fluorescent nuclear stain. EYFP and TPH expression were examined with a confocal microscope (BX61WI, Olympus).

Glial fibrillary acidic protein (GFAP) staining—Six mice received an injection of AAV1-DIO-ChR2-EYFP into the MnR, and were randomly assigned to one of two groups. Three of the mice received a 4-hour MnR photostimulation procedure (2-pulse train per 2 s when mice were immobile), while the other three received no photostimulation. Twenty-four hours later, they were intracardially perfused with ice-cold 0.9% saline followed by 4% paraformaldehyde. Brains were coronally sectioned at 40 μm and immunostained with a rabbit anti-GFAP (1:500; Product No. Z0334, DAKO) and a donkey anti-rabbit secondary antibody (1:500; Code No. 711-605-152; Jackson ImmunoResearch laboratories Inc.). Mounted sections were counterstained with DAPI. Three sections (from each mouse) with clear optic fiber track were used for quantification.

RNA *in situ* hybridization

To co-localize EYFP and GABA neurons, RNAscope 2.0 assay (Advanced Cell Diagnostics, Hayward, CA) was performed for detection of GAD in Vgat-IRES-Cre mice that had received an injection of AAV1-DIO-EYFP into the MnR. Briefly, the fresh frozen brain was embedded in cryo-embedding medium (OCT) and then coronally sectioned at 14 μm. Mounted sections were then fixed in chill 10% neutral buffered formalin (NBF), dehydrated in graded ethanol (50%, 70% and 100%), digested with protease and followed by hybridizations with target-specific probes. Sections were counterstained with DAPI, and the images were examined with the confocal scope.

Electrodes and optetrode

A bundle of 4 or 8 tetrodes was coupled with the movable (screw-driven) microdrive assembly (~1 g weight; Supplementary Fig. 1a, b). The MnR probe consisted of 8 tetrodes, while CA1 probe consisted of 4 tetrodes. Each tetrode consisted of four wires (90% platinum and 10% iridium; 18-μm diameter with an impedance of ~1–2 MΩ for each wire; California Fine Wire). The optetrode consisted of an optic fiber (100-μm diameter) and 4 tetrodes glued together, and it was coupled with the movable microdrive (Fig. 6a, b). The

distance between the tips of optical fiber and tetrodes were ~0.3–0.6 mm; the photostimulation (~10–50 mW/mm^2) was delivered with a variable interval schedule of 10–15 s.

In vivo electrophysiology

Neural signals were pre-amplified, digitized and recorded using a Neuralynx Digital Lynx acquisition system; the animals' behaviors were simultaneously recorded. Neural signals for LFP were digitized at 2 kHz and filtered at 1–500 Hz or 150–250 Hz (ripples), using ground as the reference. If no clear ripple activity was detected, the electrode array was lowered by ~80 μm daily until a clear ripple activity was detected (with the ripple amplitude reaching at least > 6 standard deviations). Spikes recorded at the hippocampal CA1 were digitized at 32 kHz and filtered at 600–6,000 Hz, using ground as the reference. Spikes recorded at the MnR were digitized at 32 kHz and filtered at 250–8,000 Hz, using one recording electrode that lacked obvious spike signals as the reference. The MnR electrode bundle was lowered by ~80 μm after a recording session. Each mouse received 3–6 recording sessions (up to 6 hours per session).

In vitro slice electrophysiology

The mice that had received an AAV1-DIO-ChR2-EYFP injection were anesthetized with isoflurane and intracardially perfused with a 30-ml ice-cold NMDG-based artificial CSF (aCSF) solution containing (in mM): 92 NMDG, 20 HEPES, 2.5 KCl, 1.2 NaH_2PO_4, 10 $MgSO_4$, 0.5 $CaCl_2$, 30 $NaHCO_3$, 25 glucose, 2 thiourea, 5 Na-ascorbate, 3 Na-pyruvate and 12 N-acetyl-L-cysteine (300–310 mOsm, pH 7.3~7.4)[51]. After perfusion, the brain was quickly removed and coronal brain slices containing the MnR were made in 250 μm with VT-1200 vibratome (Leica, Nussloch, Germany). The brain slices were then recovered for less than 15 min at 32°C in NMDG-based aCSF. After recovery, the slices were transferred and stored in room temperature HEPES-based aCSF containing (in mM): 92 NaCl, 20 HEPES, 2.5 KCl, 1.2 NaH_2PO_4, 1 $MgSO_4$, 2 $CaCl_2$, 30 $NaHCO_3$, 25 glucose, 2 thiourea, 5 Na-ascorbate, 3 Na-pyruvate and 12 N-acetyl-L-cysteine (300–310 mOsm, pH 7.3~7.4)[51]. Prior to recording, the brain slices were placed in recording chamber and superfused with standard aCSF constituted (in mM) of 125 NaCl, 2.5 KCl, 1.25 NaH_2PO_4, 1 $MgCl_2$, 2.4 $CaCl_2$, 26 $NaHCO_3$, 11 glucose, 0.1 picrotoxin, and 2 kynurenic acid, and was saturated with 95% O_2, and 5 % CO_2 at 32–34°C. To obtain a whole cell recording, glass pipette (KG-33, King Precision Glass, Claremont, CA) with pipette resistance 2.8–30 MΩ was used and filled with K^+-based internal solution containing (in mM): 140 $KMeSO_4$, 5 KCl, 0.05 EGTA, 2 $MgCl_2$, 2 Na_2ATP, 0.4 NaGTP, 10 HEPES and 0.05 Alexa Fluor 594 (Invitrogen, Carlsbad, CA), pH 7.3, 290 mOsm. Whole-cell configuration was made using a MultiClamp 700B amplifier (Molecular Devices, Sunnyvale, CA) from identified EYFP-positive cell in the MnR slice. A 200 ms pulse of blue (473 nm; intensity 0.3–4 mW) was delivered via a fiber optic attached to 40x lens and positioned just above the slice to test the expression of ChR2. The expression of ChR2 in the cell was confirmed by a light-induced inward current under voltage clamp. Then a train of 2 or 4 light pulses (pulse width, 3 ms; 25 Hz) were flashed above the slice under current clamp to examine the effect of light-induced depolarization on neuron excitability. Series resistance (10–30 MΩ) was continually monitored online with a –20 pA, 300 ms current injection given after every current injection

step; if the series resistance changed by > 20%, data were not included in the analysis. During the recording, signal was sampled at 20k Hz and filtered at 10k Hz. Data were acquired in Clampex 10.3 (Molecular Devices, Forster city, CA), and was analyzed off-line in Clampfit 10.3 (Molecular Devices, Forster city, CA) and IGOR Pro 6.0 (WaveMetrics, Lake Oswego, OR).

Fear conditioning and optical stimulation procedures

The fear conditioning experiment used 11 mice per group; this number is generally considered sufficient for behavioral study. Mice were randomly assigned into 2 groups, which received the ChR2-EYFP and EYFP-Control virus injections, respectively, and were kept on a 12 h light/dark cycle (lights on at 06:00 A.M.). Pairs of mice, consisting of an experimental (ChR2-EYFP) mouse and a control (EYFP only) mouse, had gone through the following procedure at the same time in two separate chambers. The assignments of the experimental and control mice between the two chambers were counterbalanced among pairs; thus although the experiment was not a blind one, it was conducted in a highly systematic manner. Each day's session started at 1:30 P.M. On days 1 and 2, each mouse was handled for 10–15 min. On days 3–5, mice were habituated to the photostimulation environment (~60 dB white noise background; ~23°C room temperature) and procedure without actual stimulation. Each homecage (30×20×20 cm) containing a mouse was placed under a video camera, and the mouse was connected with optic fiber cable for 4 hours. On day 5 before the stimulation habituation session, mice were also habituated to the conditioning chamber (32×25×25 cm) encased in a sound-attenuated box, by leaving them there for 10 min. On day 6, mice received single-trial contextual fear conditioning: they were allowed to freely explore the conditioning chamber for 3 min, followed by one foot-shock (0.8 mA; scrambled; 2 s). Thirty seconds after the foot-shock, mice were placed back to their homecages under a video camera and connected with the optical fiber. They received 2-pulse trains of optical stimulation (25 Hz; pulse width, 3ms; laser power, 16 mW) when the video-tracking system (EthoVision tracking system, Noldus Inc.) detected that they were immobile (rest/sleep) for 2 s, and this procedure lasted for 4 hours. On day 7, each mouse was placed in the conditioning chamber for 5 min, and their freezing response was assessed with the video-tracking software VideoFreeze (Med-Associates Inc.) with the previously established criteria[52] of animals' motion index ≤ 18 and lasted for at least 1 s (30 frames per s). Freezing scores of the computerized system were verified by a human rater blind to the manipulation (inter-rater correlation coefficient, R = 0.875, n = 22). All injection sites and optical fiber placements were verified histologically in the tested mice (n = 11 per group; Supplementary Fig. 8) and no mouse was excluded from analysis.

Electrophysiological Data Analyses

Key analyses on electrophysiological data were based on the sample size of 191 MnR neurons from 6 mice. These numbers are generally considered as sufficient in conducting statistical analyses.

Spikes—We used multiple spike-sorting parameters (e.g., principle component analysis, energy analysis) of Plexon OfflineSorter to isolate recorded spikes. Sorted spikes were processed and analyzed in NeuroExplorer (Nex Technologies) and Matlab (Mathworks,

Inc.). Low-frequency firing neurons of 0.2 Hz or less were excluded from the study's analyses due to insufficient number of spikes.

Ripples—Ripples were band-pass filtered at 150–250 Hz and analyzed with Matlab. A ripple event was defined as waves with the highest peak amplitude exceeding 6 standard deviations, plus two additional peaks exceeding 3 standard deviations and occurring within ± 30 ms of the highest peak.

SWS and REM sleep—SWS and REM sleep stages were determined by the theta (6–10 Hz)/delta (1–4 Hz) ratio extracted from the power spectrograms (Supplementary Fig. 10) when mice stayed immobile for 5 min or longer in their homecage's cardboard box filled with cotton fiber material (Nestlets™), i.e., "bed", where they exclusively slept (Supplementary Fig. 1d,e). A ratio of 2 or greater was identified as REM, while a ratio of 1 or lower was identified as SWS. Only REM/SWS sleep stages lasted for 30 s or longer were used for further analysis.

Serotoninergic neurons—We defined putative serotoninergic neurons on the basis of inter-spike interval (ISI), as previously described[53,54]. ISIs of each neuron (recorded for 1 hour or longer) were plotted on a histogram with the bin of 10 ms. Some neurons displayed only tonic activity; thus, these neurons had a single histogram peak. The latency value of the histogram peak was determined as its ISI (e.g.,Supplementary Fig. 2d). On the other hand, others displayed both tonic and high-frequency activity, which sometimes have 2 clear histogram peaks. We assigned the 2nd peak as their ISI. Neurons with the ISI longer than 200 ms were defined as putative serotonergic neurons (Supplementary Fig. 2f).

Non-serotonergic type-I and type-II neurons—Firing rate changes were determined by sorting the data of non-serotonergic neural firing with respect to ripple events using a peri-event analysis (Neuroexplorer). A 3-bin Gaussian filter was then used to smooth the peri-ripple histogram (bin = 10 ms; averaged over 1000 ripple events). Neurons that with 3 or more consecutive bins (within ± 1 s from ripple peak) differ from the baseline (a 2-s period that occurred between 2 and 4 s prior to ripple peak) by z-score of 3.28 or greater were defined as ripple-correlated neurons. These ripple-correlated neurons were classified into two types: Type-I neurons are defined as neurons that decreased firing rate by 20% or greater from the baseline, lasting 1 s or longer prior to ripple peak (Supplementary Fig. 2g); and the rest of the ripple-correlated neurons were classified as type-II.

Rates and synchrony of type-I neuron firing during ripple events—For analyses shown in Fig. 2e–g, type-I neuron and ripple event histograms (bin = 50 ms) were first smoothed with a Gaussian filter (filter width, 250 ms). Type-I neuron firing-frequency was averaged every 500-ms epoch; ripple event frequency was averaged between 0–1, 1–2, 2–3, and 3–4 s after each 500-ms epoch of the type-I neuron. Firing rates of type-I neurons were classified into 3 levels with respect to change from the baseline firing-rates for analyses shown in Supplementary Figure 6c,d. Type-I neuron's rates were high, medium, and low, if firing rates exceeds 2-fold of mean firing-frequency, fall between half and 2-fold of the mean, or fall below half-fold of the mean, respectively. Moreover, firing-synchrony of type-I neurons were classified into 3 levels for Supplementary Figure 6e,f. Type-I neuron's

synchrony were high, medium, and low, if two type-I neurons fired within a time window of 25 ms, 25.1–200 ms, or 200.1 ms or longer, respectively. The medium-synchrony time window (25–200 ms) were further divided into 25–50, 50–100 and 100–200 ms windows for analyses in Fig. 3e,f. Synchrony between type-I neurons was determined significant if 3 or more consecutive bins from the cross-correlation histogram (bin = 5 ms) exceed the z-score of 3.28 ($P < 0.001$, Wilcoxon signed rank test).

Histology for implantation verification

At the completion of the electrophysiology recordings, the final electrode position was marked by passing a 20-s, 10-μA current using a linear constant current stimulus isolator (Neurolog System) through two selected tetrodes. Mice were deeply anesthetized and intracardially perfused with ice-cold PBS followed by 4% paraformaldehyde (PFA). Brains were then removed and post-fixed in PFA for at least 24 h. Brains were rapidly frozen and sliced on a cryostat (50-μm coronal sections). Sections from the dual-site recording mice were stained with cresyl violet for microscopic examination of electrode placements, while other sections were mounted with the Mowiol mounting medium mixed with DAPI (Vector Laboratories) for fluorescent microscopic examination of viral vector expression and optical fiber placements.

Statistical analyses

Sample sizes were based on the authors' experience, previous similar studies and preliminary experiments performed in our lab. To determine firing-rate change, the value that deviates from the baseline mean by z-score of 3.28 or more was considered to be significant. Since distributions of baseline data were not necessarily normal, Wilcoxon signed-rank tests were performed on z-score-indicated changes, to assure that firing-rate changes are significant at $P < 0.001$. To determine the latency of stimulation-evoked neural activity change, the firing-rate value that deviates from the baseline mean by z-score of 1.96 or more was considered significant (Supplementary Fig. 7b). Wilcoxon signed-rank tests were used for comparisons of firing rates between two conditions (Supplementary Fig. 6c–f), and significance level was set at $P = 0.001$. Shapiro-Wilk test confirmed normality assumption for *t*-tests (Fig. 7f; Supplementary Fig. 9b), significance level was set at $P = 0.05$. When Mauchly's test detected violation of the sphericity assumption for repeated measures of ANOVAs (Fig. 4e; Supplementary Fig. 9d), the degrees of freedom for respective tests were adjusted with the Greenhouse–Geisser method. Tukey's honestly significant difference post-hoc test was performed when appropriate. All statistical tests were two-sided.

Supplementary Material

Refer to Web version on PubMed Central for supplementary material.

Acknowledgments

We thank the NIDA OTTC for producing AAVs, Evan Deneris for providing the ePet-Cre mouse line, Roger Cachope, Joe Cheer, Carlos Mejias-Aponte, Marisela Moralas, Andrew Kesner, Anton Ilango, Chen Yang, David Nguyen and Maansi Vatsan for technical assistance, and Shih-Chieh Lin, Yavin Shaham, Geoffery Schoenbaum

and Alan Saul for reading and critical discussions. The Intramural Research Program of NIDA supported the present research.

References

1. Squire LR. Memory and the hippocampus: A synthesis from findings with rats, monkeys, and humans. Psychological review. 1992; 99:195–231. [PubMed: 1594723]
2. Eichenbaum H. A cortical-hippocampal system for declarative memory. Nature Reviews Neuroscience. 2000; 1:41–50. [PubMed: 11252767]
3. Buzsaki G. Two-stage model of memory trace formation: A role for 'noisy' brain states. Neuroscience. 1989; 31:551–570. [PubMed: 2687720]
4. Ylinen A, et al. Sharp wave-associated high-frequency oscillation (200 Hz) in the intact hippocampus: network and intracellular mechanisms. The Journal of neuroscience: the official journal of the Society for Neuroscience. 1995; 15:30–46. [PubMed: 7823136]
5. Stark E, et al. Pyramidal cell-interneuron interactions underlie hippocampal ripple oscillations. Neuron. 2014; 83:467–480.10.1016/j.neuron.2014.06.023 [PubMed: 25033186]
6. Girardeau G, Zugaro M. Hippocampal ripples and memory consolidation. Current opinion in neurobiology. 2011; 21:452–459.10.1016/j.conb.2011.02.005 [PubMed: 21371881]
7. Wilson MA, McNaughton BL. Reactivation of hippocampal ensemble memories during sleep. Science. 1994; 265:676–679. [PubMed: 8036517]
8. Pavlides C, Winson J. Influences of hippocampal place cell firing in the awake state on the activity of these cells during subsequent sleep episodes. The Journal of neuroscience: the official journal of the Society for Neuroscience. 1989; 9:2907–2918. [PubMed: 2769370]
9. Nadasdy Z, Hirase H, Czurko A, Csicsvari J, Buzsaki G. Replay and time compression of recurring spike sequences in the hippocampus. The Journal of neuroscience: the official journal of the Society for Neuroscience. 1999; 19:9497–9507. [PubMed: 10531452]
10. Jadhav SP, Kemere C, German PW, Frank LM. Awake hippocampal sharp-wave ripples support spatial memory. Science. 2012; 336:1454–1458.10.1126/science.1217230 [PubMed: 22555434]
11. Ego-Stengel V, Wilson MA. Disruption of ripple-associated hippocampal activity during rest impairs spatial learning in the rat. Hippocampus. 2010; 20:1–10. [PubMed: 19816984]
12. Girardeau G, Benchenane K, Wiener SI, Buzsáki G, Zugaro MB. Selective suppression of hippocampal ripples impairs spatial memory. Nature Neuroscience. 2009; 12:1222–1223. [PubMed: 19749750]
13. Buzsaki G. Hippocampal sharp waves: Their origin and significance. Brain Research. 1986; 398:242–252. [PubMed: 3026567]
14. Buzsaki G, Leung LW, Vanderwolf CH. Cellular bases of hippocampal EEG in the behaving rat. Brain research. 1983; 287:139–171. [PubMed: 6357356]
15. Logothetis NK, et al. Hippocampal-cortical interaction during periods of subcortical silence. Nature. 2012; 491:547–553.10.1038/Nature11618 [PubMed: 23172213]
16. Ikemoto S. Brain reward circuitry beyond the mesolimbic dopamine system: A neurobiological theory. Neuroscience and Biobehavioral Reviews. 2010; 35:129–150.10.1016/j.neubiorev.2010.02.001 [PubMed: 20149820]
17. Azmitia EC, Segal M. An autoradiographic analysis of the different ascending projections of the dorsal and median raphe nuclei in the rat. Journal of Comparative Neurology. 1978; 179:641–667. [PubMed: 565370]
18. Vertes RP, Fortin WJ, Crane AM. Projections of the median raphe nucleus in the rat. Journal of Comparative Neurology. 1999; 407:555–582.10.1002/(sici)1096-9861(19990517)407:4<555::aid-cne7>3.0.co;2-e [PubMed: 10235645]
19. Varga V, et al. Fast Synaptic Subcortical Control of Hippocampal Circuits. Science. 2009; 326:449–453.10.1126/science.1178307 [PubMed: 19833972]
20. Acsády L, Arabadzisz D, Katona I, Freund TF. Topographic distribution of dorsal and median raphe neurons with hippocampal, septal and dual projection. Acta Biologica Hungarica. 1996; 47:9–19. [PubMed: 9124016]

21. Vertes RP, Kocsis B. Brainstem-diencephalo-septohippocampal systems controlling the theta rhythm of the hippocampus. Neuroscience. 1997; 81:893–926. [PubMed: 9330355]
22. Vertes RP. Hippocampal theta rhythm: A tag for short-term memory. Hippocampus. 2005; 15:923–935. [PubMed: 16149083]
23. Varga V, Sik A, Freund TF, Kocsis B. GABAB receptors in the median raphe nucleus: Distribution and role in the serotonergic control of hippocampal activity. Neuroscience. 2002; 109:119–132.10.1016/s0306-4522(01)00448-1 [PubMed: 11784704]
24. Jackson J, Bland BH, Antle MC. Nonserotonergic projection neurons in the midbrain raphe nuclei contain the vesicular glutamate transporter VGLUT3. Synapse. 2009; 63:31–41.10.1002/syn.20581 [PubMed: 18925658]
25. Kohler C, Steinbusch H. Identification of serotonin and non-serotonin-containing neurons of the mid-brain raphe projecting to the entorhinal area and the hippocampal formation. A combined immunohistochemical and fluorescent retrograde tracing study in the rat brain. Neuroscience. 1982; 7:951–975. [PubMed: 7048127]
26. Scott MM, et al. A genetic approach to access serotonin neurons for in vivo and in vitro studies. Proceedings of the National Academy of Sciences of the United States of America. 2005; 102:16472–16477.10.1073/pnas.0504510102 [PubMed: 16251278]
27. Vong L, et al. Leptin action on GABAergic neurons prevents obesity and reduces inhibitory tone to POMC neurons. Neuron. 2011; 71:142–154.10.1016/j.neuron.2011.05.028 [PubMed: 21745644]
28. Girardeau G, Benchenane K, Wiener SI, Buzsaki G, Zugaro MB. Selective suppression of hippocampal ripples impairs spatial memory. Nature neuroscience. 2009; 12:1222–1223.10.1038/Nn.2384 [PubMed: 19749750]
29. Phillips RG, Ledoux JE. Differential Contribution of Amygdala and Hippocampus to Cued and Contextual Fear Conditioning. Behavioral neuroscience. 1992; 106:274–285.10.1037//0735-7044.106.2.274 [PubMed: 1590953]
30. Kim JJ, Fanselow MS. Modality-Specific Retrograde-Amnesia of Fear. Science. 1992; 256:675–677.10.1126/science.1585183 [PubMed: 1585183]
31. Freund TF, Gulyás AI, Acsády L, Görcs T, Tóth K. Serotonergic control of the hippocampus via local inhibitory interneurons. Proceedings of the National Academy of Sciences of the United States of America. 1990; 87:8501–8505. [PubMed: 1700433]
32. Gras C, et al. A Third Vesicular Glutamate Transporter Expressed by Cholinergic and Serotoninergic Neurons. The Journal of Neuroscience. 2002; 22:5442–5451. [PubMed: 12097496]
33. Somogyi J, et al. GABAergic basket cells expressing cholecystokinin contain vesicular glutamate transporter type 3 (VGLUT3) in their synaptic terminals in hippocampus and isocortex of the rat. European Journal of Neuroscience. 2004; 19:552–569.10.1111/j.0953-816X.2003.03091.x [PubMed: 14984406]
34. Szönyi A, et al. The ascending median raphe projections are mainly glutamatergic in the mouse forebrain. Brain Structure and Function. 2014
35. Maviel T, Durkin TP, Menzaghi F, Bontempi B. Sites of Neocortical Reorganization Critical for Remote Spatial Memory. Science. 2004; 305:96–99.10.1126/science.1098180 [PubMed: 15232109]
36. Quinn JJ, Ma QD, Tinsley MR, Koch C, Fanselow MS. Inverse temporal contributions of the dorsal hippocampus and medial prefrontal cortex to the expression of long-term fear memories. Learning & Memory. 2008; 15:368–372.10.1101/lm.813608 [PubMed: 18441294]
37. Steriade M, Timofeev I. Neuronal plasticity in thalamocortical networks during sleep and waking oscillations. Neuron. 2003; 37:563–576. [PubMed: 12597855]
38. Vertes RP. Interactions among the medial prefrontal cortex, hippocampus and midline thalamus in emotional and cognitive processing in the rat. Neuroscience. 2006; 142:1–20. [PubMed: 16887277]
39. Siapas AG, Wilson MA. Coordinated interactions between hippocampal ripples and cortical spindles during slow-wave sleep. Neuron. 1998; 21:1123–1128.10.1016/S0896-6273(00)80629-7 [PubMed: 9856467]
40. Hoover WB, Vertes RP. Anatomical analysis of afferent projections to the medial prefrontal cortex in the rat. Brain Structure and Function. 2007; 212:149–179. [PubMed: 17717690]

41. Assaf SY, Miller JJ. The role of a raphe serotonin system in the control of septal unit activity and hippocampal desynchronization. Neuroscience. 1978; 3:539–550. [PubMed: 151244]
42. Macadar AW, Chalupa LM, Lindsley DB. Differentiation of brain stem loci which affect hippocampal and neocortical electrical activity. Experimental Neurology. 1974; 43:499–514. [PubMed: 4597133]
43. Maru E, Takahashi LK, Iwahara S. Effects of median raphe nucleus lesions on hippocampal EEG in the freely moving rat. Brain Research. 1979; 163:223–234. [PubMed: 218681]
44. Yamamoto T, Watanabe S, Oishi R, Ueki S. Effects of midbrain raphe stimulation and lesion on EEG activity in rats. Brain Research Bulletin. 1979; 4:491–495. [PubMed: 314836]
45. Vertes RP. An analysis of ascending brain stem systems involved in hippocampal synchronization and desynchronization. Journal of Neurophysiology. 1981; 46:1140–1159. [PubMed: 7299451]
46. Vertes RP. Brain stem generation of the hippocampal EEG. Progress in Neurobiology. 1982; 19:159–186. [PubMed: 6131484]
47. Kinney GG, Kocsis B, Vertes RP. Injections of excitatory amino acid antagonists into the median raphe nucleus produce hippocampal theta rhythm in the urethane-anesthetized rat. Brain Research. 1994; 654:96–104.10.1016/0006-8993(94)91575-x [PubMed: 7982102]
48. Kinney GG, Kocsis B, Vertes RP. Injections of muscimol into the median raphe nucleus produce hippocampal theta rhythm in the urethane anesthetized rat. Psychopharmacology. 1995; 120:244–248.10.1007/bf02311170 [PubMed: 8524970]
49. Vertes RP, Kinney GG, Kocsis B, Fortin WJ. Pharmacological suppression of the median raphe nucleus with serotonin1A agonists, 8-OH-DPAT and buspirone, produces hippocampal theta rhythm in the rat. Neuroscience. 1994; 60:441–451. [PubMed: 8072690]
50. Kinney GG, Kocsis B, Vertes RP. Medial septal unit firing characteristics following injections of 8-OH-DPAT into the median raphe nucleus. Brain Research. 1996; 708:116–122. [PubMed: 8720866]
51. Zhao S, et al. Cell type-specific channelrhodopsin-2 transgenic mice for optogenetic dissection of neural circuitry function. Nature methods. 2011; 8:745–752. [PubMed: 21985008]
52. Anagnostaras SG, et al. Automated assessment of pavlovian conditioned freezing and shock reactivity in mice using the video freeze system. Front Behav Neurosci. 2010; 410.3389/fnbeh.2010.00158
53. Mason P. Physiological identification of pontomedullary serotonergic neurons in the rat. Journal of neurophysiology. 1997; 77:1087–1098. [PubMed: 9084584]
54. Hajos M, et al. Neurochemical identification of stereotypic burst-firing neurons in the rat dorsal raphe nucleus using juxtacellular labelling methods. European Journal of Neuroscience. 2007; 25:119–126.10.1111/j.1460-9568.2006.05276.x [PubMed: 17241273]

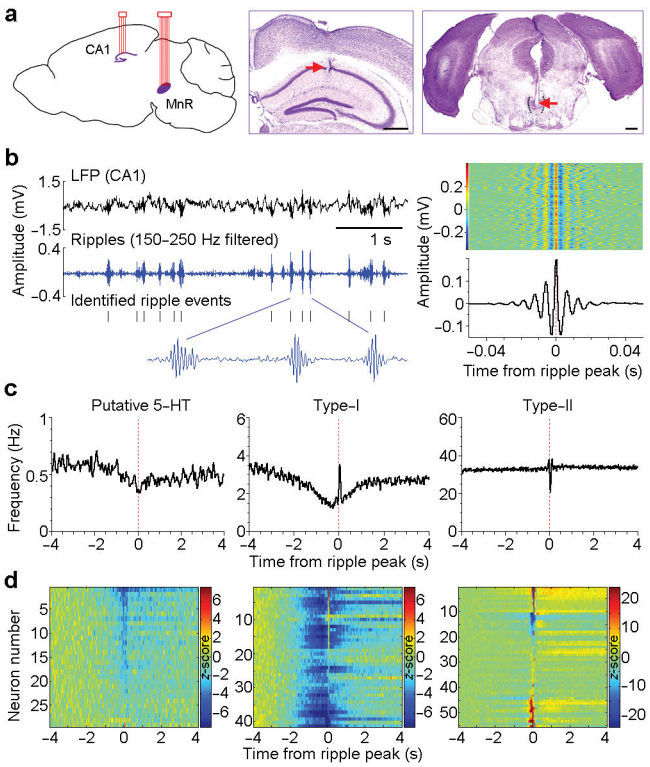

Figure 1. MnR neurons display hippocampal ripple correlated activity

(**a**), Schematic drawing of the simultaneous recording sites in the hippocampal CA1 and MnR (left panel) and representative coronal sections showing recording sites in the CA1 and MnR (middle and right panels, respectively). Dotted outline indicates boundary. Scale bars, 0.5 mm. (**b**), Representative local field potential (LFP) and filtered ripple events recorded in the CA1 (left panel), and rasters and mean amplitude of 1000 ripple events (right). Colour bar represents voltage amplitude. (**c**), Representative activity of putative 5-HT (serotonin), type-I and type-II neurons plotted in relation to the ripple peak (time 0). The 3 neurons were recorded simultaneously. (**d**), Summary of all the classified MnR neurons (recorded from 6 mice) identified as either putative 5-HT (15%, 29/191; left panel), type-I (21%, 41/191; middle panel) or type-II (29%, 55/191; right panel). Colour bars represent z-scored neural firing frequency.

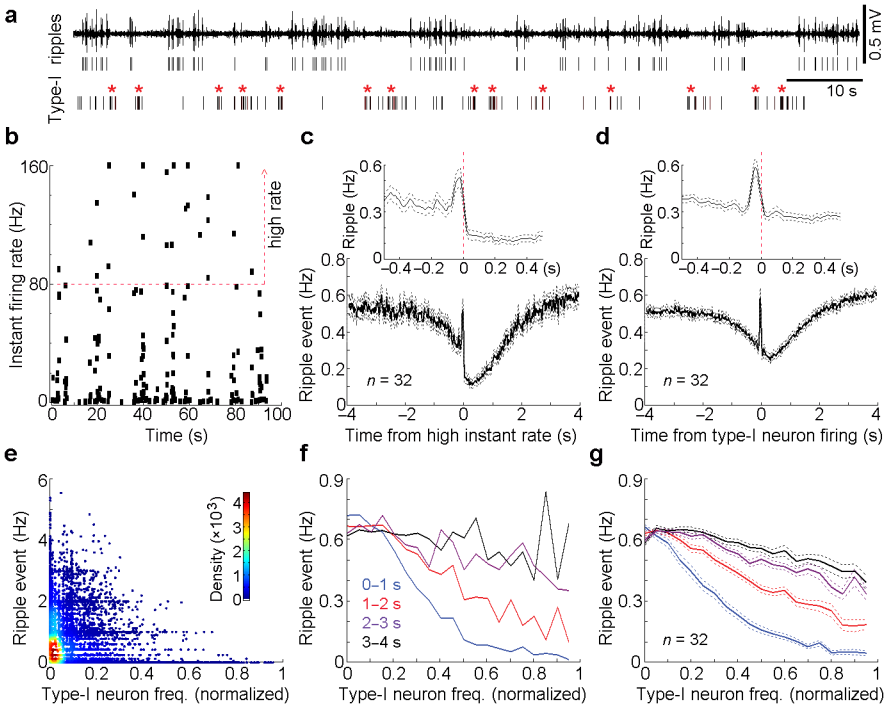

Figure 2. Ripple event frequency in relation to type-I neuron firing-frequency

(**a**), Representative filtered ripple activity, identified ripple events and spikes of a type-I MnR neuron. *High instant activity of the type-I neuron. (**b**), Instant firing rate of the same type-I neuron as shown in **a**. For this neuron, firing rates of 80 Hz or greater are classified as high instant rate of firing. (**c**), Mean ripple-event frequency (solid line) and s.e.m. (dashed) referenced to the high instant rate firing of 32 type-I neurons. Top insert panel, a finer time resolution display. (**d**) Mean cross-correlation histogram (solid line) and s.e.m. (dashed) between type-I neurons (n = 32) and ripple events. Top insert panel, a finer time resolution display. (**e**), An example of the density scatter plot of ripple event frequency *vs.* a type-I neuron firing-frequency. Type-I neuron and ripple event frequencies were first smoothed with a Gaussian filter (filter width, 250 ms). Type-I neuron firing-frequency was averaged every 500-ms epoch (represented as a dot, and ripple event frequency was calculated between 0 and 1s immediately after each 500-ms epoch of the type-I neuron). (**f**,**g**), Mean ripple event frequency as a function of type-1 neuron firing-frequency: an example of a representative neuron (**f**) and the mean ± s.e.m. of 32 neurons (**g**). Just like for the 0–1s block (**e**), ripple event frequency was calculated after each 500-ms epoch of the type-I neuron for 1–2, 2–3 and 3–4 s. Data used in **e** & **f** are from the same set of data; the last 10 highest frequencies of each type-I neuron were combined with nearby windows in **f** & **g**. Type-I neurons with mean firing-frequency above 1 Hz were used for analyses.

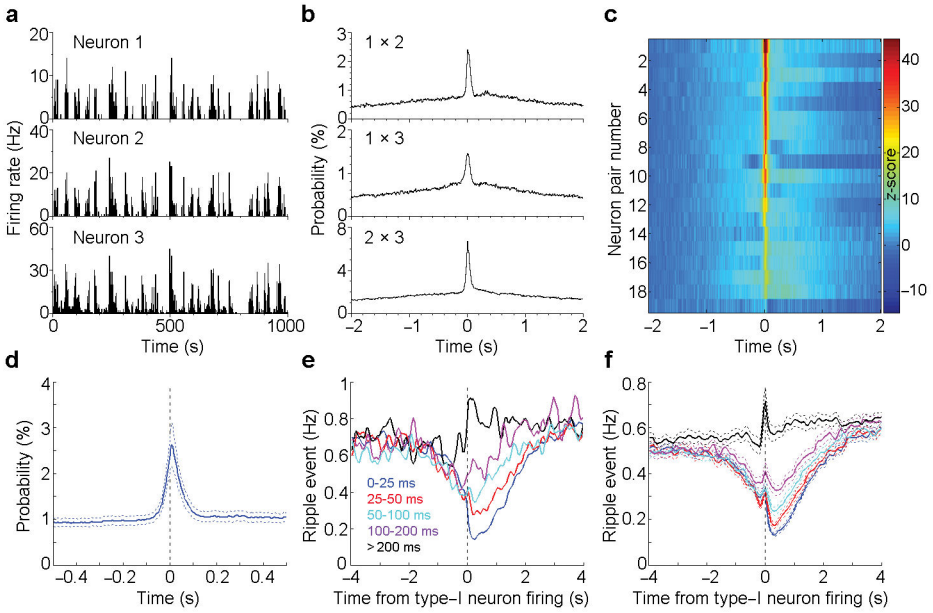

Figure 3. Ripple event frequency in relation to type-I neuron firing-synchrony

(**a**), Rate histograms of 3 simultaneously recorded type-I MnR neurons during sleep. (**b**), Cross-correlation histograms between neurons 1 & 2, 1 & 3 and 2 & 3 (the same 3 neurons as shown in **a**). (**c**), Summary of the cross-correlations for all the recorded type-I neural pairs (*n* = 19 pairs). Colour bar represents z-scored correlation probability. (**d**), Averaged cross-correlation histogram of the simultaneously recorded type-I neuron pairs (the same 19 pairs as shown in **c**). (**e**,**f**), Ripple event frequency in relation to type-I neuron synchrony window: an example of a neuron (**e**) and mean ± s.e.m. of 26 neurons (**f**). Co-firing interval was determined between two neurons by examining each spike of a type-I neuron with respect to the closest spike of another type-I neurons, and was classified into one of 5 windows: 0–25, 25–50, 50–100, 100–200, >200 ms. Type-I neurons with mean firing-frequency above 1 Hz were used for analyses.

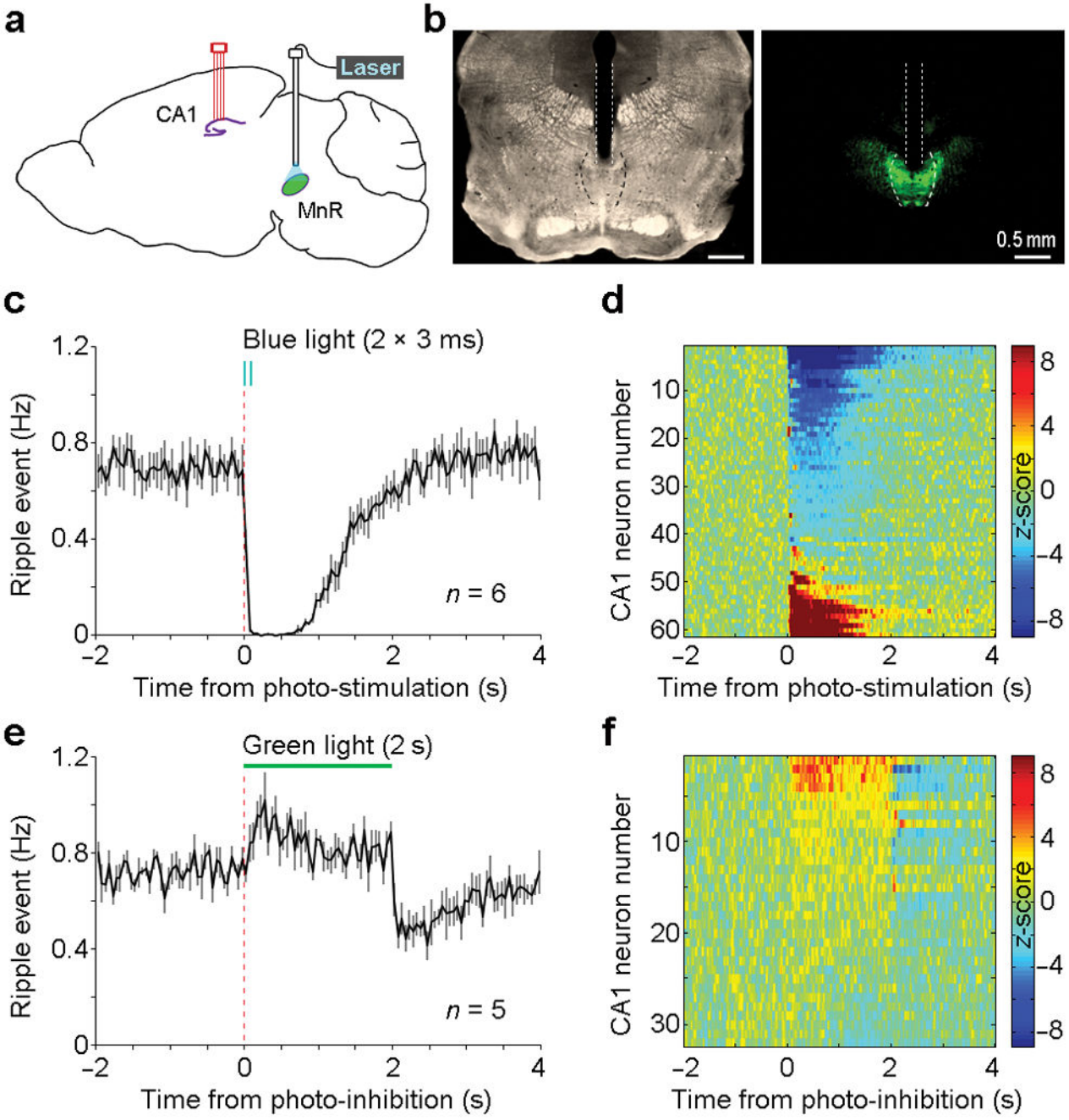

Figure 4. Up- and down-regulation of hippocampal ripple activity by the MnR

(**a**), Schematic drawing of the recording site in the hippocampal CA1 and the photostimulation site in the MnR. (**b**), A representative coronal section showing the optical fiber track (left panel) and EYFP expression (right panel). Dotted lines and outlines indicate the optical fiber track and the boundary of MnR, respectively. (**c**,**e**), Mean ripple-event frequency (solid line) and s.e.m. (error bars) upon MnR photostimulation (**c**; 2 pulses at 25 Hz; pulse width, 3 ms) and photoinhibition (**e**; 2 s). (**d**,**f**), Mean firing frequency of all the

recorded CA1 neurons upon MnR photostimulation (**d**; $n = 61$) and photoinhibition (**f**; $n = 32$). Colour bars represent z-scored neural firing frequency.

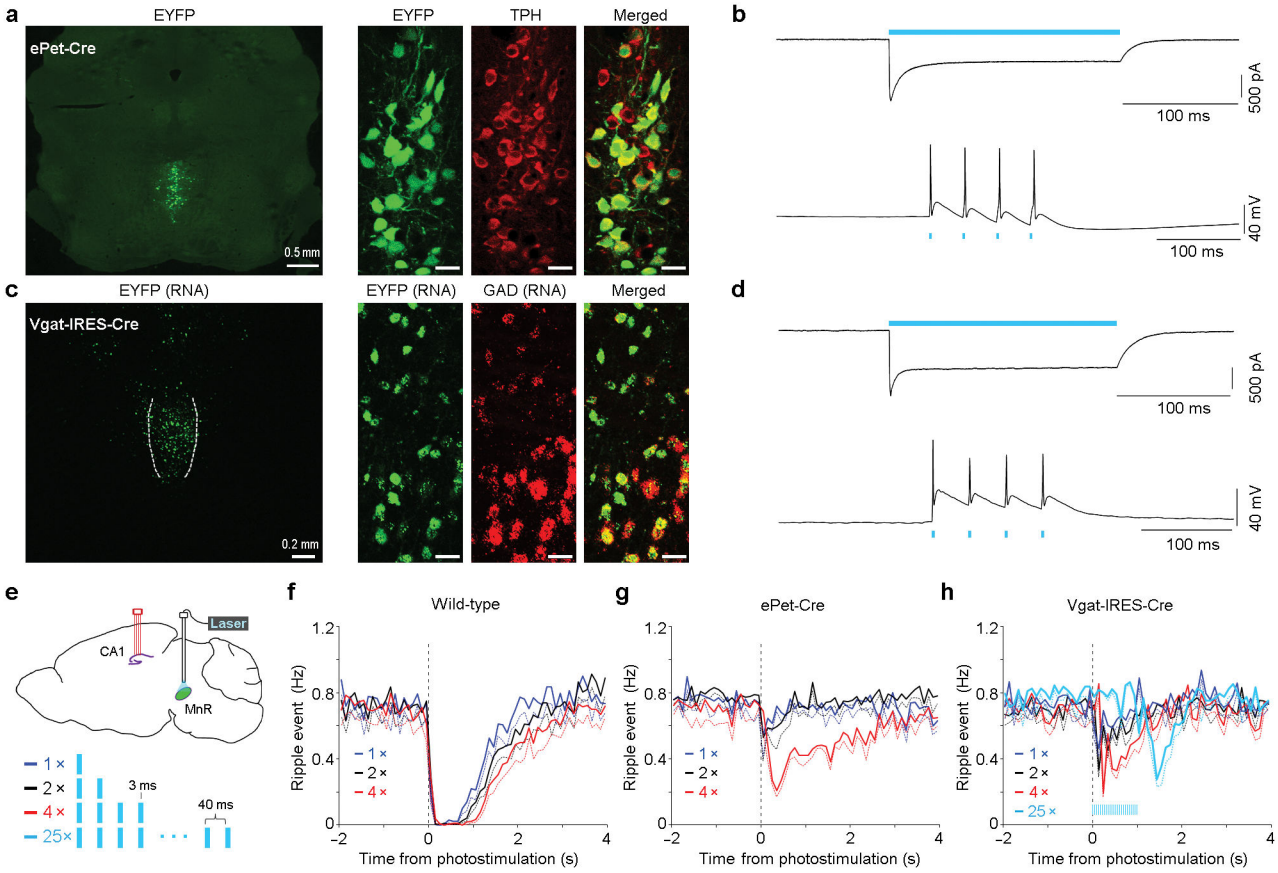

Figure 5. Subtypes of MnR neurons in regulation of hippocampal ripple activity

(**a,c**), Representative coronal sections showing co-localizations of EYFP with tryptophan hydroxylase (TPH) in ePet-Cre mice (**a**) and glutamic acid decarboxylase (GAD) in Vgat-IRES-Cre mice (**c**). Scale bars in the right panels, 20 μm. (**b,d**), Representative voltage (top panels) and current (bottom panels) clamps of putative serotonergic neurons (**b**) and GABAergic neurons (**d**). (**e**), Schematic experiment design and photostimulation parameters. **f**-(**h**), Mean ripple-event frequency (solid line) and s.e.m. (dashed) upon 1, 2 and 4 pulses of MnR photostimulation. The extent of suppression of ripple activity was examined as a function of pulse number in wild-type (n = 6), ePet-Cre (n = 4) and Vgat-IRES-Cre (n = 4) mice. Photostimulation was delivered with a variable interval of 5–15 s during immobility. Light trains of 1-, 2- and 4-pulses were similarly effective in wild-type mice. In ePet-Cre mice, trains of 4 pulses evoked stronger suppression of ripple activity than 1- or 2-pulse trains. In Vgat-IRES-Cre mice, although trains of 1-, 2- or 4-pulses had small effects, ripple activity tended to be suppressed at the offset of photostimulation. To clarify whether ripple activity is suppressed at the offset of GABAergic neuron stimulation, we examined effects of a longer stimulation train (25 pulses; lasting 1 s), and confirmed a rebound suppression of ripple activity upon the offset of the 25-pulse photostimulation (light blue lines shown in **h**).

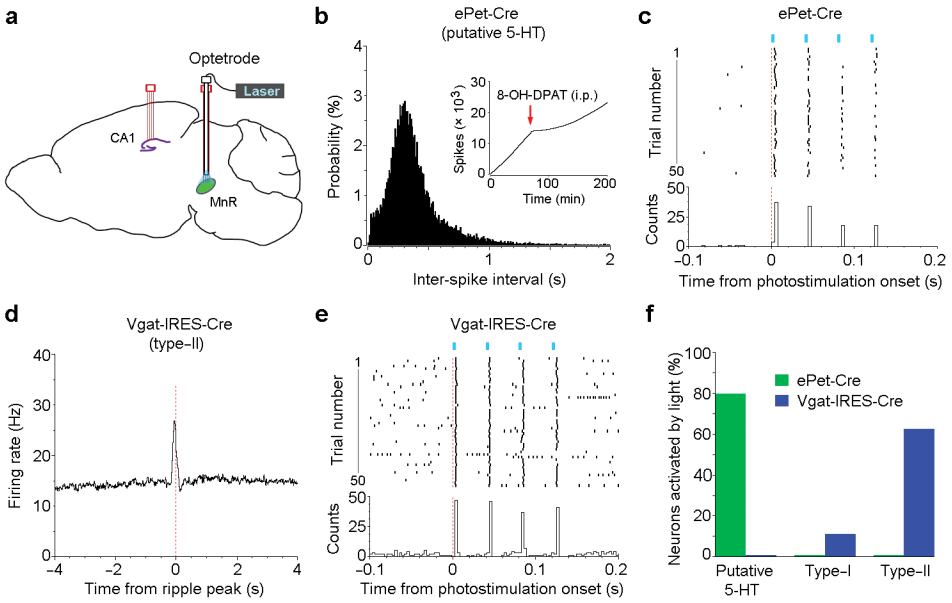

Figure 6. Optical tagging of the MnR serotonergic and GABAergic neurons

(**a**), Schematic drawing showing a 4-tetrode probe in the hippocampal CA1 and a MnR optetrode consisting of an optic fiber and 4 tetrodes. ePet-Cre (*n* = 4) and Vgat-IRES-Cre (*n* = 3) mice received these implants and an injection of AAV-DIO-ChR2-EYFP into the MnR for the identification of serotonergic and GABAergic neurons, respectively. (**b**)**,** Inter-spike interval histogram of a putative serotonergic neuron identified by optogenetic stimulation. Inserted panel (**b**) shows cumulative spikes of the same neuron after an injection of the serotonin 1A receptor agonist 8-OH-DPAT (0.2 mg/kg, i.p.). **(d**), Peri-ripple event histogram of a putative GABAergic neuron identified by optogenetic stimulation. (**c,e**)**,** Peri-event rasters and histogram of the same 2 neurons (as shown in **b** and **d)** upon 4-pulse light trains (25 Hz; pulse width, 3 ms). (**f**)**,** Percentages of putative 5-HT (*n* = 5 and 8 from ePet-Cre and Vgat-IRES-Cre mice, respectively), type-I (*n* = 6 and 9, respectively) and type-II (*n* = 16 and 8, respectively) neurons that responded to photostimulation. Neurons are considered to be responsible to photostimulation if peri-stimulation histogram bin with the z-score of 3.28 ($P < 0.001$) or greater occurs within 5 ms from the onset of photostimulation. Response latencies varied between 2 and 5 ms.

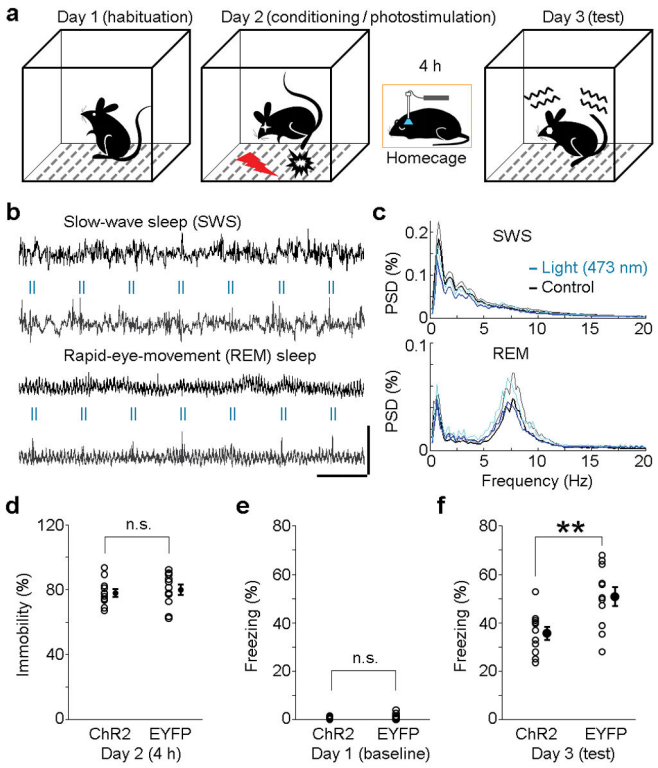

Figure 7. Impairment of fear memory consolidation by MnR photostimulation

(**a**), Contextual fear conditioning protocol. On day 2 immediately after fear conditioning, mice were returned to the homecage where they received 2-pulse trains of MnR photostimulation (25 Hz; pulse width, 3 ms) if they were immobile over the course of 4 hours. (**b**), Representative hippocampal CA1 LFP during SWS and REM sleep with and without MnR photostimulation. Scale bars, 2 s and 2 mW. (**c**), Mean power spectral density (PSD, black and dark-blue lines) and s.d. (grey and light-blue) with (light- and dark-blue lines) and without (grey and black lines) MnR photostimulation during SWS or REM sleep (n = 17 and 20 sessions, respectively). (**d**), Percentage of immobility time for individual mice during the 4-h stimulation session following fear conditioning (n = 11 per group). **e, f**, Percentage of freezing time for individual mice before and after fear conditioning (n = 11 per group; ***P* = 0.0042, unpaired t-test). Error bars indicate s.e.m. in **d** and **f.**